CHEMISTRY
A EUROPEAN JOURNAL

ChemPubSoc
Europe

DOI: 10.1002/chem.201302241

Spin-Crossover Complex on Au(111): Structural and Electronic Differences Between Mono- and Multilayers

Thiruvancheril G. Gopakumar,[a] Matthias Bernien,[b] Holger Naggert,[c] Francesca Matino,[a] Christian F. Hermanns,[b] Alexander Bannwarth,[c] Svenja Mühlenberend,[a] Alex Krüger,[b] Dennis Krüger,[b] Fabian Nickel,[b] Waldemar Walter,[b] Richard Berndt,*[a] Wolfgang Kuch,*[b] and Felix Tuczek*[c]

Abstract: Submono-, mono- and multilayers of the Fe(II) spin-crossover (SCO) complex $[Fe(bpz)_2(phen)]$ (bpz=dihydrobis(pyrazolyl)borate, phen=1,10-phenanthroline) have been prepared by vacuum deposition on Au(111) substrates and investigated with near edge X-ray absorption fine structure (NEXAFS) spectroscopy and scanning tunneling microscopy (STM). As evidenced by NEXAFS, molecules of the second layer exhibit a thermal spin crossover transition, although with a more gradual characteristics than in the bulk. For mono- and submonolayers of $[Fe(bpz)_2(phen)]$ deposited on Au(111) substrates at room temperature both NEXAFS and STM indicate a dissociation of $[Fe(bpz)_2(phen)]$ on Au(111) into four-coordinate complexes, $[Fe(bpz)_2]$, and phen molecules. Keeping the gold substrate at elevated temperatures ordered monolayers of intact molecules of $[Fe(bpz)_2(phen)]$ are formed which can be spin-switched by electron-induced excited spin-state trapping (ELIESST).

Keywords: iron · gold · scanning tunnel microscopy · spintronics · spin crossover · X-ray absorption spectroscopy

Introduction

The spin state of transition-metal complexes is determined by the central atom, its oxidation state, and the type of ligands. In spin-crossover (SCO) complexes, the ligands have moderate ligand-field strengths, and therefore, the metal atom may possess different spin states at comparable energies, which can be occupied as a function of temperature. Importantly, these spin states can also be changed by external stimuli, such as light, pressure, or magnetic field.[1–10] Alternative spin-switching mechanisms in transition-metal complexes involve change of coordination number[11–14] or conformation[15–16] and charging the ligands coordinated to the metal center.[17] The large number of possibilities to manipulate the spin state underscores the prominent role of spin-switchable complexes in the area of molecular switches.

To date, spin-state switching of SCO complexes has mostly been demonstrated in powder samples.[1,18,19] An attractive option with respect to possible applications is to prepare spin-crossover systems as thin films. Following this idea, Langmuir–Blodgett films,[20] self-assembled monolayers,[21] and spin-coated[22] films of SCO complexes have been investigated. To obtain high-quality thin films of SCO complexes, which may be incorporated into devices,[2] it is desirable to prepare them by vacuum deposition.[23–29] A detailed structural characterization of these systems is necessary, because even small structural changes of the deposited SCO molecules may strongly alter their properties in comparison to the bulk, which in turn will seriously affect their capability to function as spin switches.

Herein, we investigate the structure of vacuum-deposited ultrathin films of the SCO molecule iron–bis(dihydrobis(pyrazolyl)borate)-1,10-phenanthroline, $[Fe(bpz)_2(phen)]$,[19,30,31] on Au(111), for which electron-induced excited spin-state trapping (ELIESST) has been reported recently.[24] To this end submono-, mono-, and multilayers of $[Fe(bpz)_2(phen)]$ molecules are deposited on Au(111) substrates under different conditions and characterized by using near-edge X-ray absorption fine structure (NEXAFS) spectroscopy and scanning tunneling microscopy (STM). As was shown by NEXAFS, coverage of $[Fe(bpz)_2(phen)]$ greater than one monolayer exhibits a thermal spin transition in analogy to the bulk or 400 nm thick films.[23] However, in the first layer

[a] Dr. T. G. Gopakumar,[+] Dr. F. Matino, S. Mühlenberend, Prof. Dr. R. Berndt
Institut für Experimentelle und Angewandte Physik
Christian-Albrechts-Universität zu Kiel, 24098 Kiel (Germany)
E-mail: berndt@physik.uni-kiel.de

[b] Dr. M. Bernien,[+] C. F. Hermanns, A. Krüger, D. Krüger, F. Nickel, W. Walter, Prof. Dr. W. Kuch
Institut für Experimentalphysik, Freie Universität Berlin
Arnimallee 14, 14195 Berlin (Germany)
E-mail: kuch@physik.fu-berlin.de

[c] H. Naggert,[+] Dr. A. Bannwarth, Prof. Dr. F. Tuczek
Institut für Anorganische Chemie
Christian-Albrechts Universität zu Kiel, 24098 Kiel (Germany)
E-mail: ftuczek@ac.uni-kiel.de

[+] These authors contributed equally to this work.

Supporting information for this article is available on the WWW under http://dx.doi.org/10.1002/chem.201302241.

on Au(111), the data reveal a decomposition of [Fe(bpz)$_2$(phen)] into phenanthroline (phen) and iron–bis(dihydrobis(pyrazolyl)borate), [Fe(bpz)$_2$]. This was supported by STM, which shows pairs of phenanthroline molecules covering the Au(111) surface after deposition of a submonolayer of [Fe(bpz)$_2$(phen)] on a gold substrate kept at room temperature. Submonolayer vacuum deposition of this compound on a gold substrate heated to 100–150 °C, on the other hand, leads to an ordered phase of [Fe(bpz)$_2$(phen)] molecules, which can be switched reversibly between high- and low-spin (HS and LS, respectively) states by the ELIESST effect (see above).

Results and Discussion

X-ray absorption data: *Thermal and X-ray induced spin-state switching*: Thermal spin crossover of the complex [Fe(bpz)$_2$(phen)] adsorbed on Au(111) is observed if the coverage exceeds one monolayer (ML). This was indicated by NEXAFS spectra at the Fe L_3 edge of 1.6 ML deposited at room temperature, which shows clear evidence of a peak at 709.6 eV coming up at temperatures around 90 K (Figure 1 a). In accordance with X-ray absorption (XRA) measurements on similar SCO complexes,[28,29,31] this peak is associated with the LS state of the [Fe(bpz)$_2$(phen)] complex. Importantly, the relative fraction of this state is strongly reduced both at higher and lower temperatures. The reduction of the LS fraction at higher temperatures is in agreement with the thermal spin-crossover behavior of [Fe(bpz)$_2$(phen)], exhibiting a spin-transition temperature $T_{1/2}$ of 165 K.[19,30,31] The reduction of the LS fraction at lower temperatures than 90 K is associated with an excitation of the [Fe(bpz)$_2$(phen)] complex to the HS state by X-ray irradiation (see below).

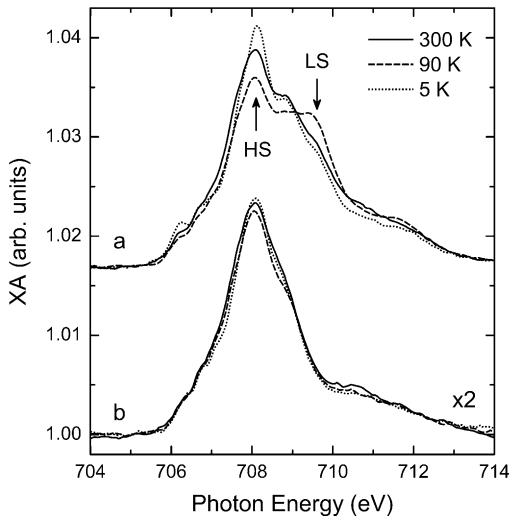

Figure 1. Isotropic Fe L_3 NEXAFS spectra recorded at the magic angle of incidence of 54.7° at 300, 90, and 5 K of a) 1.6 ML and b) 0.8 ML of [Fe(bpz)$_2$(phen)] on Au(111). Arrows indicate the energies representative of molecules in the HS and LS states.

When the coverage is below one ML, no variation of the Fe L_3 line shape with temperature was observed (Figure 1 b). This shows that between 5 and 300 K, the Fe ions are conserved in one electronic state (Fe^{II} HS, see below) at these submonolayer coverages, and that the thermal spin crossover observed in the 1.6 ML sample has to be confined to molecules in the second monolayer. Furthermore, the line shape of the monolayer spectra is different from that of the 1.6 ML sample, indicating that the electronic configurations of the Fe ions in the first and second molecular layer are different.

For a measure of the fraction of molecules in the HS state, we use the intensity ratio of the X-ray absorptions at 708.1 and 709.6 eV, which are representative for HS and LS molecules, respectively (arrows in Figure 1 a). Its variation with temperature of the 1.6 ML sample is presented in Figure 2 during both heating and cooling of the sample.

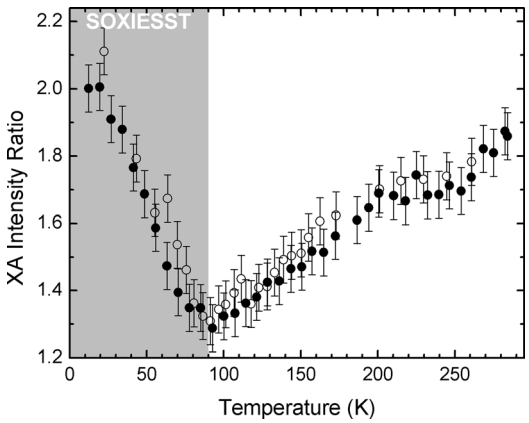

Figure 2. Fe L_3 NEXAFS intensity ratio at 708.1 and 709.6 eV photon energy plotted over temperature for cooling (○) and heating (●) the sample with a rate of 4 K min^{-1}.

Starting from ambient temperature, the intensity ratio gradually decreases towards a minimum at 90 K and then increases again at lower temperatures. The behavior above 90 K corresponds to a thermal spin-crossover transition, which is incomplete even at 300 K. We tentatively attribute the more gradual characteristics compared to the bulk material[19,23,30] to a lack of cooperative interactions, which account for steeper spin transitions in crystalline matrices. The behavior below 90 K is in contradiction to the thermal spin-crossover characteristics of [Fe(bpz)$_2$(phen)], which would correspond to a LS state in this temperature regime.[19,23,30] Radiation damage can be excluded as a possible cause, because the behavior of the spectral line shape with temperature is reversible (Figure 2). The increase of the HS fraction below 90 K thus has to be explained by soft X-ray-induced excited spin-state trapping (SOXIESST), that is, illumination by soft X-rays during the absorption measurements leads to a photon-induced transition to the HS state, as has been observed for [Fe(phen)$_2$(NCS)$_2$] molecular crystals[32]

and for thick films of $[Fe(bpz)_2(bipy)]$.[29] This effect is similar to the phenomenon of light-induced excited spin-state trapping (LIESST), in which a LS to HS transition is induced by visible light at low temperatures. For both SOXIESST and LIESST, back relaxation of the excited HS state to the LS ground state is very slow at low temperatures. Importantly, a LIESST effect has been detected in $[Fe(bpz)_2(phen)]$ between 10 and 40 K in thicker films,[23] that is, in a similar temperature interval in which in the NEXAFS experiment the SOXIESST effect is observed.

The absence of any thermally or X-ray-induced SCO switching in the submonolayer indicates that the molecules are chemically modified due to the interaction with the Au(111) substrate. As will be shown in the following sections, the $[Fe(bpz)_2(phen)]$ molecule dissociates into the four-coordinate complex $[Fe(bpz)_2]$ and phen on the Au(111) surface.

Fragmentation of $[Fe(bpz)_2(phen)]$ on gold: To probe the structure of the adsorbed iron complexes on Au(111), NEXAFS spectra of a submonolayer and a multilayer of $[Fe(pbz)_2(phen)]$ are compared in Figure 3 to spectra of the four-coordinate complex without phenanthroline, $[Fe(bpz)_2]$, prepared separately and also deposited on Au(111) by evaporation. Spectra were recorded at an angle of incidence between the X-ray wave vector and the surface of 54.7°, at which the intensity is independent of the molecular orientation.

The isotropic Fe $L_{2,3}$ spectrum of the multilayer of $[Fe(bpz)_2(phen)]$ (Figure 3a, dashed line) exhibits a pronounced multiplet structure, which is typical of an Fe^{II} HS configuration.[33] In the data of the submonolayer (dotted line), the multiplet structure is smeared out; nevertheless, the positions of the L_3 and L_2 resonances and their relative intensities are similar to the multilayer result. This indicates that the spin and the oxidation state of the Fe ions are not modified upon adsorption. The change in line shape may rather be attributed to a change of coordination. This hypothesis is supported by the fact that the data of the four-coordinate complex $[Fe(bpz)_2]$ (solid line) fully match the submonolayer data of $[Fe(bpz)_2(phen)]$, which in turn suggests that the $[Fe(bpz)_2(phen)]$ complex dissociates in the first layer on Au(111) into $[Fe(bpz)_2]$ and phen. In contrast to the six-coordinate complex $[Fe(bpz)_2(phen)]$, which exhibits spin-crossover behavior, the four-coordinate complex $[Fe(bpz)_2]$ is in the HS state at all temperatures (Figure S1 in the Supporting Information). This also explains the temperature-independent NEXAFS spectrum found for the submonolayer of $[Fe(bpz)_2(phen)]$ on Au(111) (see above, Figure 1b).

Further support for this conclusion is provided by NEXAFS data at the N *K* edge (Figure 3b). The multilayer data of $[Fe(bpz)_2(phen)]$ (dashed line) exhibit three π^* resonances at 399.1, 400.8, and 401.4 eV. Again, a similar spectrum was obtained for the submonolayer (dotted line). However, for the four-coordinate complex $[Fe(bpz)_2]$ (solid line), no peak at 399.1 eV was observed. Therefore, this feature can safely be attributed to the two nitrogen atoms of the phen ligand, which is missing in this complex. The resonances at 400.8 and 401.4 eV, on the other hand, stem from the four nitrogen atoms of the bpz ligands.

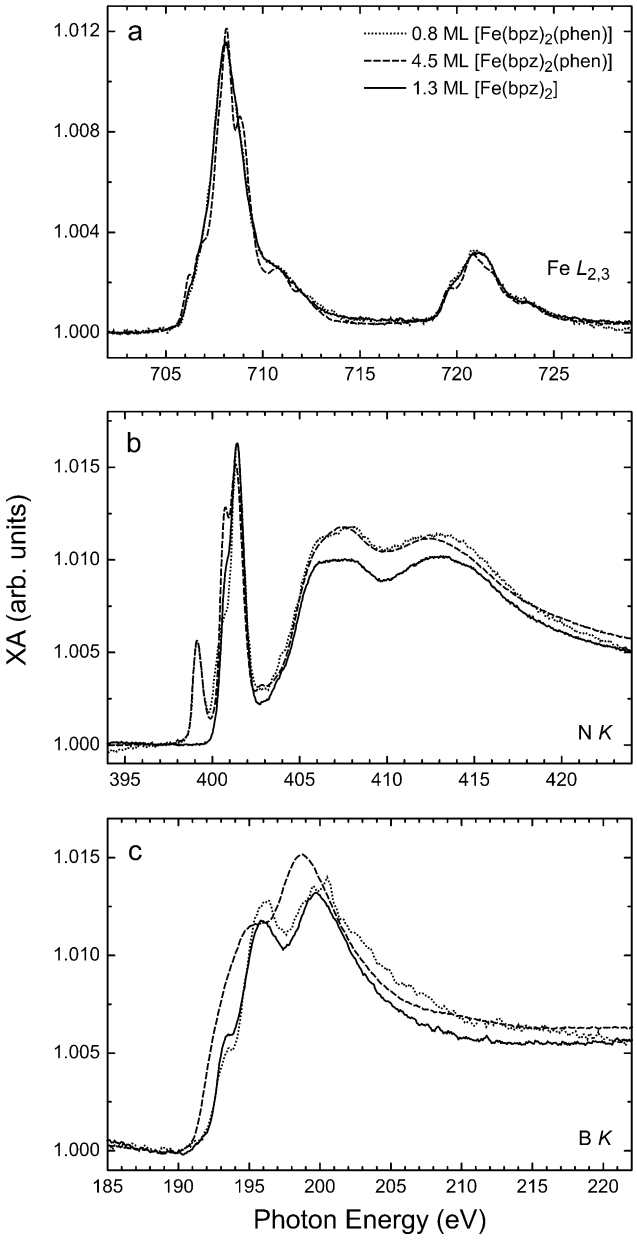

Figure 3. Isotropic NEXAFS spectra of a) iron $L_{2,3}$, b) nitrogen *K*, and c) boron *K* transitions recorded at the magic angle 54.7° at a temperature $T = 300$ K. Dotted, dashed, and solid lines indicate data from 0.8 and 4.5 ML of $[Fe(bpz)_2(phen)]$ and 1.3 ML $[Fe(bpz)_2]$, respectively, on Au(111). The latter two have been scaled down in intensity for better comparison.

Spectra of the boron *K* edge (Figure 3c) corroborate the results obtained from the iron and nitrogen edges. Also in this case, the spectra of $[Fe(bpz)_2]$ and the submonolayer of $[Fe(bpz)_2(phen)]$ are very similar, whereas for a multilayer of $[Fe(bpz)_2(phen)]$ a qualitatively different spectrum was obtained. This again indicates that fragmentation of $[Fe(bpz)_2(phen)]$ occurs when the complex is in direct contact with the Au substrate. The change of the boron XRA spectrum might thereby be induced by a direct contact between

the boron atoms and the Au surface based on an adsorption geometry of $[Fe(bpz)_2]$ inferred from STM (see below).

The similarity of the spectra of the submonolayer of $[Fe(bpz)_2(phen)]$ and $[Fe(bpz)_2]$ at all three absorption edges (besides the phen peak in the N *K* edge) thus suggests cleavage of the phenanthroline ligand as the relevant fragmentation process. As can be concluded from the presence of the π* resonance at 399.1 eV, in the N *K* spectrum of 0.8 ML $[Fe(bpz)_2(phen)]$, however, the phen ligand remains on the surface. The orientation of the phenanthroline fragment can be determined from angle-dependent N *K* NEXAFS spectra of 0.8 ML of $[Fe(bpz)_2(phen)]$ on Au(111) (Figure 4). Although the two nitrogen π* resonances of the bpz ligand only exhibit a weak angle dependence, the resonance at 399.1 eV, which is due to phen, drastically varies with the angle between the X-ray wave vector and the surface, indicating a high degree of orientation order. From a quantitative evaluation of the angle dependency, an average tilt angle of phen of $(16\pm4)°$ with respect to the surface plane was found, indicating that the molecules are lying almost flat on the surface. Such orientation again corroborates the cleavage of the phen ligand, because it is not compatible with the three-dimensional structure of the intact molecule.

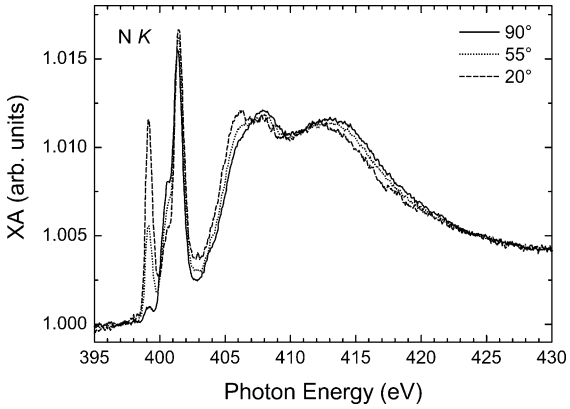

Figure 4. Angle-dependent N *K* NEXAFS spectra of 0.8 ML of $[Fe(bpz)_2(phen)]$ on Au(111) recorded with linearly p-polarized X-rays.

STM data: For a microscopic characterization, $[Fe(bpz)_2(phen)]$ and its fragments were investigated with STM under ultrahigh vacuum conditions. At ambient temperature, stable imaging of the prepared layers was not achieved. Therefore, below we only present data that were recorded at a temperature of 5 K.

Layers prepared at ambient temperature: Figure 5 displays typical STM images of surfaces prepared at ambient temperature. The overview in Figure 5a shows rather irregular molecular chains on a Au(111) surface. Closer inspection reveals that these chains are comprised of two distinct units (Figure 5b). We observe four-lobed structures and pairs of bean-shaped features (apparent heights ca. 600 and 230 pm, respectively). Based on the symmetries of these structures in the STM images, we attribute these patterns to fragments of $[Fe(bpz)_2(phen)]$, namely, four-coordinate $[Fe(bpz)_2]$ complexes and dimers of phenanthroline molecules, respectively. The lateral dimensions of the patterns are consistent with the calculated gas-phase geometries of the corresponding molecules shown in Figure 5c. Apparently, $[Fe(bpz)_2]$ adsorbs with two pyrazole groups almost parallel to the surface and the remaining two pyrazole groups pointing away from the surface (arrowheads in Figure 5c). The observed image contrast with two higher and two slightly lower lobes is expected for such a structure. Note that the boron atoms of the two bpz ligands (light grey in Figure 5c) get in close contact with the Au surface in this geometry. The above-described interpretations are further corroborated by data shown below. In addition to the fragments, which can be imaged in a reproducible fashion at low tunneling currents ($I=35$ pA), we also observed somewhat higher and unstable structures, which may be due to intact $[Fe(bpz)_2(phen)]$ molecules, although a firm statement on this issue cannot be made.

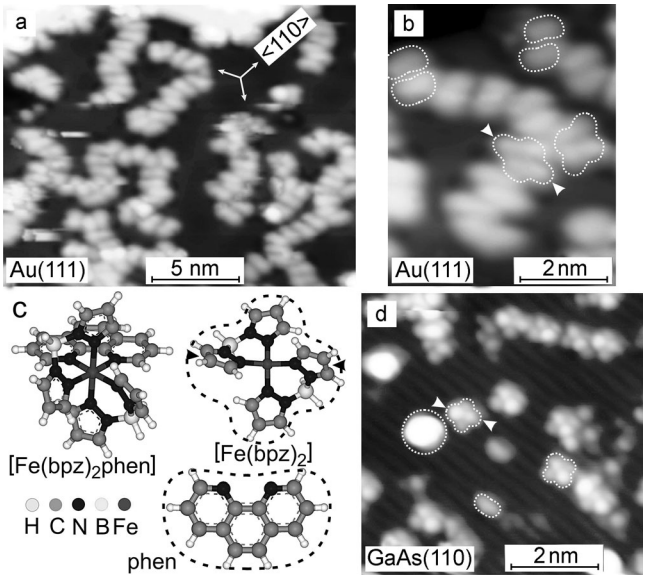

Figure 5. Constant-current STM topographs of $[Fe(bpz)_2(phen)]$ on a),b) Au(111) and d) GaAs(110) along with c) calculated structures of $[Fe(bpz)_2(phen)]$, $[Fe(bpz)_2]$, and phenanthroline (phen). Compact directions of Au(111) are indicated by arrows in a). Dotted four-lobed clover shapes depict $[Fe(bpz)_2]$ and dotted bean shapes depict phenanthroline. Arrowheads on $[Fe(bpz)_2]$ indicate the pyrazolyl ligands that are pointing away from the plane of paper. Corresponding lobes in STM images are marked with white arrowheads. One $[Fe(bpz)_2(phen)]$ molecule in d) is indicated by a circle.

To test the above-discussed interpretation, we deposited $[Fe(bpz)_2(phen)]$ on the more reactive GaAs(110) surface at room temperature. Due to its dangling bonds, this surface is expected to suppress molecular diffusion. In low-temperature STM images, three distinct species were found (Figure 5d). Two of them, a four-lobed and a bean-shaped pattern, closely resemble the data from Au(111) and thus are attributed to $[Fe(bpz)_2]$ and phenanthroline. Unlike on Au, phenanthroline molecules are found as monomers, presuma-

bly due to their drastically reduced diffusion on GaAs(110). The third species gives rise to approximately 0.5 nm high, circular protrusions. Although these protrusions exhibit some variation of their heights and shapes, spectra of the differential conductance (dI/dV) exhibit identical features (STS in the Supporting Information, Figure S2 b). Therefore, we tentatively attribute this species to intact [Fe(bpz)$_2$(phen)] complexes. Taking into account a variety of surface areas, for example, the data shown in the Supporting Information Figure S2 a, we estimate that between 20 and 30 % of all molecule-related structures on GaAs are intact [Fe(bpz)$_2$(phen)] complexes.

To unambiguously verify that the bean-shaped features are indeed phenanthroline molecules, we deposited pure phenanthroline on Au(111) surfaces at room temperature. Although the STM images suffer from some instability of the molecular layer, dimers are resolved (Figure 6). Their shapes and heights (0.2 nm) match to those observed upon deposition of [Fe(bpz)$_2$(phen)] on Au(111).

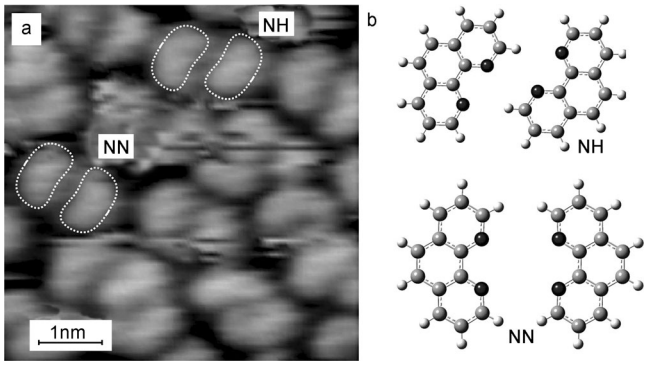

Figure 6. a) Constant current STM topograph ($V=-1.4$ V, $I=50$ pA) of phenanthroline deposited on Au(111) at ambient temperature and recorded at 5 K. Instabilities in imaging are observed quite often, presumably due to high mobility of phen. NN and NH indicate different types of phenanthroline dimers. b) Structure of NN and NH type dimers. The structure was optimized for phenanthroline confined to two dimensions but otherwise neglecting the substrate.

Layers prepared at 100 °C: When monolayer coverages of [Fe(bpz)$_2$(phen)] are deposited at higher substrate temperatures of 100–150 °C on Au(111), more regular patterns were obtained. Figure 7 a shows an overview of a 50×50 nm^2 area. Much of the surface is covered by a compact and ordered layer (A). Besides that, less ordered areas with a lower density of features (B) were found.

A high-resolution image of the ordered structure A is displayed in Figure 7 b. We have previously analyzed the image contrast and attributed it to intact [Fe(bpz)$_2$(phen)] molecules.[24] The nearly threefold symmetry of the molecular pattern, the spectroscopic features of the molecule, and the demonstration of reversible switching between a HS and a LS state are clear evidences for this assignment. Molecules in adjacent rows are marked by triangles with the thick side representing the pyrazole groups of a single bpz ligand (see

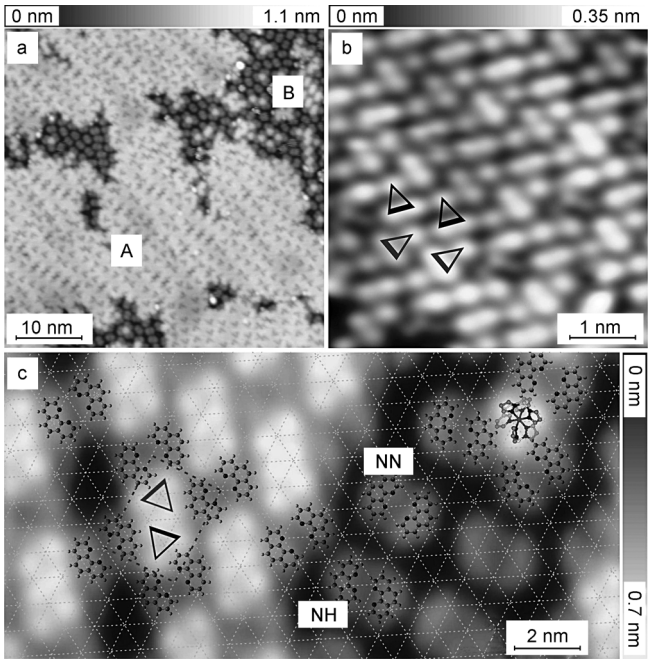

Figure 7. Constant-current STM topographs ($V=-1.3$ V, $I=50$ pA) of [Fe(bpz)$_2$(phen)] deposited on Au(111) at 100–150 °C substrate temperature. a) Different types of packing are visible. "A" marks a dense array of [Fe(bpz)$_2$(phen)], "B" a loosely packed mixture of phenanthroline dimers and [Fe(bpz)$_2$(phen)]. b) High-resolution image of phase A. Triangles depict some [Fe(bpz)$_2$(phen)] molecules. c) High-resolution image of phase B and phenanthroline dimers. A dashed grid depicts the Au(111) surface mesh. Some [Fe(bpz)$_2$(phen)] molecules are depicted by triangles. NN and NH represent two types of phenanthroline dimers. Close to [Fe(bpz)$_2$(phen)] molecules in phase B phenanthroline dimers are ordered with a unit cell indicated by a dashed rectangle.

above); the triangles are rotated by approximately 66° with respect to each other.[24]

Figure 7 c shows a less dense area (type B) at higher resolution. Again, dimers of bean-shaped phenanthroline were observed. Closer inspection revealed two types of dimers, which are labeled NN and NH. These dimers differ by the relative orientation of the two phenanthroline molecules. In the NN type, the nitrogen atoms of the phenanthroline moieties face each other, whereas in the NH type nitrogen atoms of one molecule face hydrogen atoms of the other. Given that the NH type is energetically more favorable by 7.1 kcal mol^{-1} (ca. 0.3 eV) in the gas phase, the abundance of NN is remarkable (for details, see the Figure S3 in the Supporting Information). This effect is most likely due to the interaction of N with the Au substrate atoms. Figure 7 c also shows the optimized geometries of NN and NH dimers overlaid on the scaled STM image along with a grid representing the surface mesh of Au(111). The nitrogen atoms of NN dimers show a perfect registry with Au(111) bridge sites or top sites. In contrast, for NH, no registry with the Au lattice is discernible.

In a previous report,[24] the bean-shaped features were interpreted as being due to intact [Fe(bpz)$_2$(phen)] with an inverted orientation. Based on the present detailed NEXAFS

and STM data, this model has to be revised. Significant fragmentation of the adsorbed molecules occurs. The bean-shaped features are in fact due to phenanthroline dimers, as was evidenced by imaging surfaces that had been exposed to the phenanthroline alone.

In less densely packed areas (e.g., Figure 7c), the concentration of phenanthroline dimers is high. Therefore, we considered the possibility that the entire surface may be covered with dimers, and intact [Fe(bpz)$_2$(phen)] is located on top of such a layer. However, this scenario appears to be unlikely. In the top right corner of Figure 7c, a single [Fe(bpz)$_2$(phen)] molecule is surrounded by three phenanthroline dimers. Models of the latter molecules are overlaid. From the lateral dimensions of the dimers, it is clear that there is not enough space for a dimer underneath the [Fe(bpz)$_2$(phen)] molecule. A similar conclusion is reached for the structures in the left half of the image. We observe pairs of intact [Fe(bpz)$_2$(phen)] complexes that are surrounded by phenanthroline dimers. These dimers do not leave enough space for a dimer underneath each of the [Fe(bpz)$_2$(phen)]. It should be noted that in both structures, the presence of a single phenanthroline underneath [Fe(bpz)$_2$(phen)] cannot be excluded. As to the apparent heights of [Fe(bpz)$_2$(phen)] with respect to the Au(111) substrate, we observed essentially identical values (650 pm) from single [Fe(bpz)$_2$(phen)] molecules, from pairs of these complexes, and from molecules in the densely packed structure of Figure 7a. This indicates that the height of [Fe(bpz)$_2$(phen)] with respect to the substrate is most likely identical in these three cases.

STM images of layers prepared at 100 °C did not show clearly resolved features that could be attributed to [Fe(bpz)$_2$], which was found to be rather abundant in the films prepared at ambient temperature. However, a rather trivial reason may account for this observation. On all surfaces prepared, stable imaging was possible only in some areas. The missing [Fe(bpz)$_2$] may have aggregated in the less stable areas and thus have escaped detection.

Finally, we demonstrate switching of the spin state of [Fe(bpz)$_2$(phen)] in the ordered, low-density structure of Figure 7c. The procedure is identical to the one presented in Ref. [24]. Figure 8 shows a sequence of STM images. Because the spin-transition temperature of free [Fe(bpz)$_2$(phen)] is approximately 165 K (Figure S1 in the Supporting Information),[19,23,30] molecules imaged at 5 K are expected to be in a LS state. Switching to HS is induced by increasing the sample voltage to $V=3$ V at an arbitrary molecule (circle in Figure 8a) for a sub-second time interval while maintaining the tip-sample distance constant. A subsequent STM image (Figure 8b) reveals six molecules (indicated by arrows) at remote locations, the apparent height of which has increased by approximately 200–300 pm depending on the sample bias polarity. This drastic change reflects the modified electronic structure of the HS state.[24]

Notably, the switching from LS to HS occurs for molecules in a nanometer distance from the position of the STM tip. This "remote" switching process is analogous to the case of DMSO on Au(111), in which hot electrons injected from the tip are laterally transported by surface resonances at the Au(111) surface, inducing dissociation over distances up to 100 nm from the injection point.[34] As an alternative explanation, a field-induced process has been considered.[35,36] However, this mechanism was not found to be compatible with the experimental findings on our system.[24] In contrast to the LS→HS switching, the reverse process may be selectively induced on a given HS molecule (marked with dashed circles in Figure 8c and d) with $V=1.6$ V, demonstrating again the presence of single-molecule spin-state switching in the ordered monolayers of [Fe(bpz)$_2$(phen)] on Au(111).

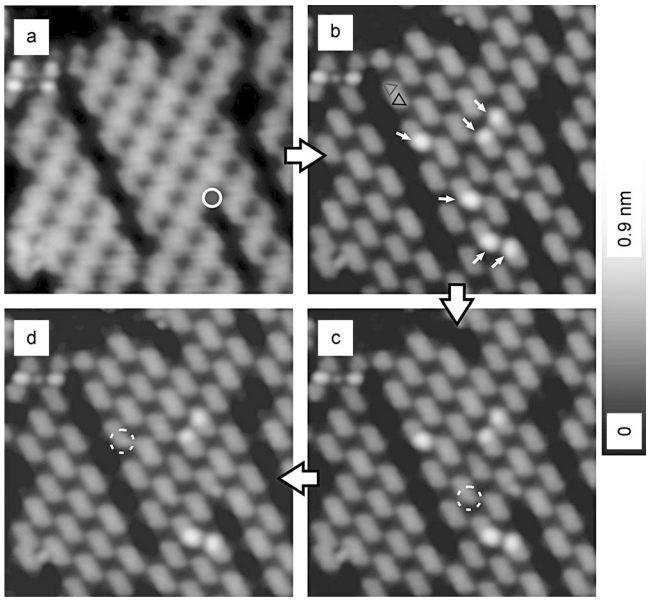

Figure 8. Constant-current STM topographs ($V=-1.5$ V, $I=50$ pA) of phase B of [Fe(bpz)$_2$(phen)] on Au(111). A voltage pulse (2.8 V) was applied at the position indicated by a circle in a). The consecutive image b) shows six bright molecules labeled by arrows. These bright molecules are assigned to the high-spin state of [Fe(bpz)$_2$(phen)].[24] The following frames c) and d) show switching of single molecules (depicted by dashed circles) from the HS state to the original LS state.

Conclusion

In the preceding sections, NEXAFS and STM have been employed to investigate ultrathin films of [Fe(bpz)$_2$(phen)] complexes deposited on Au(111) surfaces by vapor deposition in UHV. As was evidenced by NEXAFS, molecules of the second layer exhibited a thermal spin-crossover transition, although with more gradual characteristics compared to the bulk material. This behavior of our ultrathin films most probably is due to a lack of cooperative interactions,[23] which in crystalline matrices account for the steep spin-transition curves observed experimentally. Below 90 K, excitation to the high-spin state is mediated by the SOXIESST effect, which is in agreement with other examples reported in the literature.

All of the described properties are absent for the first monolayer and submonolayers of [Fe(bpz)$_2$(phen)] deposit-

ed on Au(111) substrates at room temperature. As was evidenced by NEXAFS, these molecules exhibited a different electronic structure compared to that of the intact six-coordinate complex, which in addition is not temperature dependent. Combined evidence from NEXAFS and STM indicates that upon adsorption of [Fe(bpz)$_2$(phen)] on a Au(111) substrate kept at room temperature, this molecule dissociates into a four-coordinate complex, [Fe(bpz)$_2$], and a phen molecule, which is lying flat on the surface. For the [Fe(bpz)$_2$] complex, which is quasi-tetrahedral in the gas phase, an adsorption geometry is proposed, in which two of the pyrazole moieties are parallel to the surface, whereas the two other pyrazole moieties are perpendicular to the surface, giving rise to four-lobed clover-shaped structures in the STM. In this structure, the boron atoms of the two bpz ligands get in close contact with the gold surface, which accounts for the drastic change in the boron NEXAFS spectrum upon going from a multilayer to a submonolayer of [Fe(bpz)$_2$(phen)] and to the four-coordinate complex [Fe(bpz)$_2$], respectively.

Remarkably, the observed fragmentation process represents the reversal of the synthetic procedure, by which [Fe(bpz)$_2$(phen)] is prepared, that is, reaction of [Fe(bpz)$_2$] with phen. As was found experimentally, surface-deposited [Fe(bpz)$_2$] can also react with phen in a solid-state reaction to form [Fe(bpz)$_2$(phen)] (Figure S4 in the Supporting Information). On the other hand, thermal analysis (DTA-TG) of [Fe(bpz)$_2$(phen)], phen, and [K(bpz)] with concomitant mass spectrometric detection (Figure S5 a and b in the Supporting Information) show that [Fe(bpz)$_2$(phen)] should be intact in the gas phase and thus also support a surface-induced ligand-dissociation process. We speculate that a similar scenario might also occur in the related compound [Fe(bpz)$_2$(bipy)] when directly adsorbed on Au(111). The remaining change of NEXAFS spectra reported for a submonolayer of this system[29] might then be ascribed to molecules already adsorbing in the second layer. For thicker vacuum-deposited films of [Fe(bpz)$_2$(phen)] and [Fe(bpz)$_2$(bipy)] (400–500 nm), the properties of the bulk material are observed.[23] XRD data of vacuum-deposited multilayers of the latter compound also showed the pattern of the bulk material.[37]

STM investigations on ultrathin films of [Fe(bpz)$_2$(phen)] prepared at ambient and elevated substrate temperatures on Au and GaAs support the fragmentation of the complex evidenced by NEXAFS. The phenanthroline fragments form two types of dimers, which are stabilized by hydrogen bridges and interaction with substrate atoms. At elevated temperatures, ordered monolayers of intact molecules are obtained, which gives rise to a quasi-threefold pattern originating from the bis(pyrazolyl)borate ligands. In these ordered structures, single-molecule spin-state switching can be induced by the ELIESST effect, as was first reported in Ref. [24].

Experimental Section

[Fe(bpz)$_2$(phen)] was synthesized as was described previously.[18] [Fe(bpz)$_2$] was obtained according to the procedure reported in Ref. [38].

Sample preparation was carried out in ultrahigh vacuum with a base pressure of 5×10^{-10} mbar. The Au(111) substrate was prepared by repeated sputtering and annealing cycles. [Fe(bpz)$_2$(phen)] was evaporated from a Knudsen cell at about 160 °C and deposited onto the substrate held at RT, as well as at about 130 °C. [Fe(bpz)$_2$] was deposited at about 120 °C onto the substrate held at RT. For the NEXAFS experiments, coverages were estimated by using a quartz microbalance and the absolute Fe L_3 resonance intensity (see the Supporting Information, section 6).

X-ray absorption experiments have been performed at the beam lines PM3 (0.8 ML [Fe(bpz)$_2$(phen)]; Figures 3 and 4), UE56/2 PGM1 (4.5 ML [Fe(bpz)$_2$(phen)] and 1.3 ML [Fe(bpz)$_2$]; Figure 3), and UE46 PGM1 (Figures 1 and 2) at BESSY II. For all three beam lines, the photon flux density was in the range of approximately 10^{13} photons s^{-1} cm^{-2}, whereas the spot size of the X-rays on the sample was approximately 0.15 mm^2, approximately 0.25 mm^2, and approximately 0.50 mm^2, respectively. Energy resolutions were set to approximately 150 meV, approximately 200 meV, and approximately 300 meV at the C-*K*, N-*K*, and Fe-$L_{2,3}$ edges, respectively, except for the Fe L_3 spectra recorded at the UE46 PGM1 at approximately 150 meV. Spectra were recorded by total electron yield measurements and normalized to a gold-grid reference signal, as well as to the corresponding spectra of the substrate without adsorbed molecules. For the measurements at the UE46 PGM1, the signal of the last refocusing mirror was used as reference. Besides the reversible LS to HS conversion due to the SOXIESST effect, no irreversible time-dependent modifications of the NEXAFS spectra were observed. We thus can exclude the importance of radiation-damage effects for the presented measurements. Isotropic spectra were recorded with linearly p-polarized X-rays at the magic angle of incidence, that is, 54.7° between the *k* vector of the X rays and the surface, at which the NEXAFS resonance intensities are independent of the orientations of the molecular orbitals.

Acknowledgements

E. Weschke is acknowledged for his support, W. Mahler and T. Kachel for their technical support during the beam times. Financial funding is gratefully acknowledged by the DFG through Sfb 677 and 658.

[1] *Spin Crossover in Transition Metal Compounds I-III* (Eds.: P. Gütlich, H. A. Goodwin), Springer, Berlin **2004**.
[2] H. J. Shepherd, G. Molnár, W. Nicolazzi, L. Salmon, A. Bousseksou, *Eur. J. Inorg. Chem.* **2013**, 5–6.
[3] A. Hauser, *Top. Curr. Chem.* **2004**, *234*, 155–198.
[4] E. König, K. Madeja, *Inorg. Chem.* **1967**, *6*, 48–55.
[5] P. Ganguli, P. Gütlich, E. W. Müller, *Inorg. Chem.* **1982**, *21*, 3429–3433.
[6] O. Kahn, C. J. Martinez, *Science* **1998**, *279*, 44–48.
[7] S. Decurtins, P. Gütlich, C. P. Köhler, H. Spiering, *J. Chem. Soc. Chem. Commun.* **1985**, 430–432.
[8] P. Gütlich, A. Hauser, H. Spiering, *Angew. Chem.* **1994**, *106*, 2109–2141; *Angew. Chem. Int. Ed. Engl.* **1994**, *33*, 2024–2054.
[9] V. Ksenofontov, A. B. Gaspar, G. Levchenko, B. Fitzsimmons, P. Gütlich, *J. Phys. Chem. B* **2004**, *108*, 7723–7727.
[10] A. Bousseksou, G. Molnár, J.-P. Tuchagues, N. Menéndez, É. Codjovi, F. Varret, *C. R. Chim.* **2003**, *6*, 329–335.
[11] S. Thies, H. Sell, C. Bornholdt, C. Schütt, F. Köhler, F. Tuczek, R. Herges, *Chem. Eur. J.* **2012**, *18*, 16358–16368.
[12] S. Venkataramani, U. Jana, M. Dommaschk, F. D. Sönnichsen, F. Tuczek, R. Herges, *Science* **2011**, *331*, 445–448.

[13] W. Hieringer, K. Flechtner, A. Kretschmann, K. Seufert, W. Auwärter, J. V. Barth, A. Görling, H. Steinrück, J. M. Gottfried, *J. Am. Chem. Soc.* **2011**, *133*, 6206–6222.
[14] T. Komeda, H. Isshiki, J. Liu, Y.-F. Zhang, N. Lorente, K. Katoh, B. K. Breedlove, M. Yamashita, *Nat. Commun.* **2011**, *2*, 217.
[15] T. Choi, S. Bedwani, A. Rochefort, C.-Y. Chen, A. J. Epstein, J. A. Gupta, *Nano Lett.* **2010**, *10*, 4175–4180.
[16] J. J. Parks, A. R. Champagne, T. A. Costi, W. W. Shum, A. N. Pasupathy, E. Neuscamman, S. Flores-Torres, P. S. Cornaglia, A. A. Aligia, C. A. Balseiro, G. K.-L. Chan, H. D. Abruña, D. C. Ralph, *Science* **2010**, *328*, 1370–1373.
[17] V. Meded, A. Bagrets, K. Fink, R. Chandrasekar, M. Ruben, F. Evers, A. Bernand-Mantel, J. S. Seldenthuis, A. Beukman, H. S. J. van der Zant, *Phys. Rev. B* **2011**, *83*, 245415.
[18] P. Gütlich, A. B. Gaspar, Y. Garcia, *Beilstein J. Org. Chem.* **2013**, *9*, 342–391.
[19] J. A. Real, M. C. Muñoz, J. Faus, X. Solans, *Inorg. Chem.* **1997**, *36*, 3008–3013.
[20] H. Soyer, C. Mingotaud, M. L. Boillot, P. Delhaes, *Langmuir* **1998**, *14*, 5890–5895.
[21] M. Ruben, J. Rojo, F. J. R. Salguero, L. H. Uppadine, J. M. Lehn, *Angew. Chem.* **2004**, *116*, 3728–3747; *Angew. Chem. Int. Ed.* **2004**, *43*, 3644–3662.
[22] M. Matsuda, H. Tajima, *Chem. Lett.* **2007**, *36*, 700–701.
[23] H. Naggert, A. Bannwarth, S. Chemnitz, Th. v. Hofe, E. Quandt, F. Tuczek, *Dalton Trans.* **2011**, *40*, 6364–6366.
[24] a) T. G. Gopakumar, F. Matino, H. Naggert, A. Bannwarth, F. Tuczek, R. Berndt, *Angew. Chem. Int. Ed.* **2012**, *51*, 6262–6266; b) T. G. Gopakumar, F. Matino, H. Naggert, A. Bannwarth, F. Tuczek, R. Berndt, *Angew. Chem. Int. Ed.* **2013**, *52*, 3796.
[25] S. Shi, G. Schmerber, J. Arabski, J.-B. Beaufrand, D. J. Kim, S. Boukari, M. Bowen, N. T. Kemp, N. Viart, G. Rogez, E. Beaurepaire, H. Aubriet, J. Petersen, *Appl. Phys. Lett.* **2009**, *95*, 043303.
[26] T. Miyamachi, M. Gruber, V. Davesne, M. Bowen, S. Boukari, L. Joly, F. Scheurer, G. Rogez, T. K. Yamada, P. Ohresser, E. Beaurepaire, W. Wulfhekel, *Nat. Commun.* **2012**, *3*, 938.
[27] E. C. Ellingsworth, B. Turner, G. Szulczewski, *RSC Adv.* **2013**, *3*, 3745–3754.
[28] M. Bernien, D. Wiedemann, C. F. Hermanns, A. Krüger, D. Rolf, W. Kroener, P. Müller, A. Grohmann, W. Kuch, *J. Phys. Chem. Lett.* **2012**, *3*, 3431–3434.
[29] B. Warner, J. C. Oberg, T. G. Gill, F. El Hallak, C. F. Hirjibehedin, M. Serri, S. Heutz, M.-A. Arrio, P. Sainctavit, M. Mannini, G. Poneti, R. Sessoli, P. Rosa, *J. Phys. Chem. Lett.* **2013**, *4*, 1546–1552.
[30] N. Moliner, L. Salmon, L. Capes, M. C. Muñoz, J.-F. Létard, A. Bousseksou, J.-P. Tuchagues, J. J. McGarvey, A. C. Dennis, M. Castro, R. Burriel, J. A. Real, *J. Phys. Chem. B* **2002**, *106*, 4276–4283.
[31] C. Cartier dit Moulin, P. Rudolf, A. M. Flank, C. T. Chen, *J. Phys. Chem.* **1992**, *96*, 6196–6198.
[32] D. Collison, C. D. Garner, C. M. McGrath, J. F. W. Mosselmans, M. D. Roper, J. M. W. Seddon, E. Sinn, N. A. Young, *Dalton Trans.* **1997**, 4371–4376.
[33] T. Palamarciuc, J. C. Oberg, F. E. Hallak, C. F. Hirjibehedin, M. Serri, S. Heutz, J.-F. Létard, P. Rosa, *J. Mater. Chem.* **2012**, *22*, 9690–9695.
[34] M. Maksymovych, D. B. Dougherty, X.-Y. Zhu, J. T. Yates Jr., *Phys. Rev. Lett.* **2007**, *99*, 016101.
[35] N. Baadji, M. Piacenza, T. Tugsuz, F. Della Sala, G. Maruccio, S. Sanvito, *Nat. Mater.* **2009**, *8*, 813–817.
[36] M. Kepenekian, B. Le Guennic, V. Robert, *Phys. Rev. B* **2009**, *79*, 094428.
[37] X. Zhang, T. Palamarciuc, P. Rosa, J.-F. Létard, B. Doudin, Z. Z. Zhang, J. Wang, P. A. Dowben, *J. Phys. Chem. C* **2012**, *116*, 23291–23296.
[38] S. Trofimenko, *Inorg. Chem.* **1967**, *6*, 3170–3177.

Received: June 13, 2013
Published online: October 7, 2013

